Controlling magnetic and electric dipole modes in hollow silicon nanocylinders

Marie Anne van de Haar, Jorik van de Groep, Benjamin J.M. Brenny and Albert Polman*

Center for Nanophotonics, FOM Institute AMOLF, Science Park 104, 1098 XG, Amsterdam, the Netherlands

*polman@amolf.nl

Abstract: We propose a dielectric nanoresonator geometry consisting of hollow dielectric nanocylinders which support geometrical resonances. We fabricate such hollow Si particles with an outer diameter of 108–251 nm on a Si substrate, and determine their resonant modes with cathodoluminescence (CL) spectroscopy and optical dark-field (DF) scattering measurements. The scattering behavior is numerically investigated in a systematic fashion as a function of wavelength and particle geometry. We find that the additional design parameter as a result of the introduction of a center gap can be used to control the relative spectral spacing of the resonant modes, which will enable additional control over the angular radiation pattern of the scatterers. Furthermore, the gap offers direct access to the enhanced magnetic dipole modal field in the center of the particle.

OCIS codes: (220.4241) Nanostructure fabrication, (230.5750) Resonators, (290.5850) Scattering, particles, (290.5820) Scattering measurements.

References and links

1. C. F. Bohren and D. R. Huffman, *Absorption and Scattering of Light by Small Particles* (Wiley-VCH Verlag GmbH, 1983).
2. J. A. Schuller and M. L. Brongersma, "General properties of dielectric optical antennas," Opt. Express **17**, 24084–24095 (2009).
3. J. van de Groep and A. Polman, "Designing dielectric resonators on substrates: Combining magnetic and electric resonances," Opt. Express **21**, 26285–26302 (2013).
4. J. Grandidier, D. M. Callahan, J. N. Munday, and H. A. Atwater, "Light absorption enhancement in thin-film solar cells using whispering gallery modes in dielectric nanospheres," Adv. Mater. **23**, 1272–1276 (2011).
5. A. Raman, Z. Yu, and S. Fan, "Dielectric nanostructures for broadband light trapping in organic solar cells," Opt. Express **19**, 19015–19026 (2011).
6. S. A. Mann, R. R. Grote, R. M. Osgood, and J. A. Schuller, "Dielectric particle and void resonators for thin film solar cell textures," Opt. Express **19**, 25729–25740 (2011).
7. P. Spinelli, M. A. Verschuuren, and A. Polman, "Broadband omnidirectional antireflection coating based on subwavelength surface mie resonators," Nat. Commun. **3**, 692 (2012).
8. A. P. Vasudev, J. A. Schuller, and M. L. Brongersma, "Nanophotonic light trapping with patterned transparent conductive oxides," Opt. Express **20**, A385–A394 (2012).
9. C. van Lare, F. Lenzmann, M. A. Verschuuren, and A. Polman, "Dielectric scattering patterns for efficient light trapping in thin-film solar cells," Nano Lett. **15**, 4846–4852 (2015).
10. L. Cao, J. S. White, J.-S. Park, J. A. Schuller, B. M. Clemens, and M. L. Brongersma, "Engineering light absorption in semiconductor nanowire devices," Nat. Mater. **8**, 643–647 (2009).
11. L. Cao, J.-S. Park, P. Fan, B. Clemens, and M. L. Brongersma, "Resonant germanium nanoantenna photodetectors," Nano Lett. **10**, 1229–1233 (2010).
12. R. Yan, J.-H. Park, Y. Choi, C.-J. Heo, S.-M. Yang, L. P. Lee, and P. Yang, "Nanowire-based single-cell endoscopy," Nat. Nano **7**, 191–196 (2012).

#254688 Received 27 Nov 2015; revised 15 Jan 2016; accepted 16 Jan 2016; published 26 Jan 2016

13. A. García-Etxarri, R. Gómez-Medina, L. S. Froufe-Pérez, C. López, L. Chantada, F. Scheffold, J. Aizpurua, M. Nieto-Vesperinas, and J. J. Sáenz, "Strong magnetic response of submicron silicon particles in the infrared," Opt. Express **19**, 4815–4826 (2011).
14. A. B. Evlyukhin, C. Reinhardt, A. Seidel, B. S. Luk´yanchuk, and B. N. Chichkov, "Optical response features of si-nanoparticle arrays," Phys. Rev. B **82**, 045404 (2010).
15. Y. H. Fu, A. I. Kuznetsov, A. E. Miroshnichenko, Y. F. Yu, and B. Luk´yanchuk, "Directional visible light scattering by silicon nanoparticles," Nat. Commun. **4**, 1527 (2013).
16. S. Person, M. Jain, Z. Lapin, J. J. Sáenz, G. Wicks, and L. Novotny, "Demonstration of zero optical backscattering from single nanoparticles," Nano Lett. **13**, 1806–1809 (2013).
17. I. Staude, A. E. Miroshnichenko, M. Decker, N. T. Fofang, S. Liu, E. Gonzales, J. Dominguez, T. S. Luk, D. N. Neshev, I. Brener, and Y. Kivshar, "Tailoring directional scattering through magnetic and electric resonances in subwavelength silicon nanodisks," ACS Nano **7**, 7824–7832 (2013).
18. M. Kerker, D. S. Wang, and C. L. Giles, "Electromagnetic scattering by magnetic spheres," Journal of the Optical Society of America **73**, 765–767 (1983).
19. P. P. Iyer, N. A. Butakov, and J. A. Schuller, "Reconfigurable semiconductor phased-array metasurfaces," ACS Photonics **2**, 1077–1084 (2015).
20. S. Karaveli and R. Zia, "Strong enhancement of magnetic dipole emission in a multilevel electronic system," Opt. Lett. **35**, 3318–3320 (2010).
21. B. Rolly, B. Bebey, S. Bidault, B. Stout, and N. Bonod, "Promoting magnetic dipolar transition in trivalent lanthanide ions with lossless mie resonances," Phys. Rev. B **85**, 245432 (2012).
22. R. Zia, M. D. Selker, P. B. Catrysse, and M. L. Brongersma, "Geometries and materials for subwavelength surface plasmon modes," Journal of the Optical Society of America A **21**, 2442–2446 (2004).
23. R. Hussain, S. S. Kruk, C. E. Bonner, M. A. Noginov, I. Staude, Y. S. Kivshar, N. Noginova, and D. N. Neshev, "Enhancing Eu3+ magnetic dipole emission by resonant plasmonic nanostructures," Opt. Lett. **40**, 1659–1662 (2015).
24. M. Mivelle, T. Grosjean, G. W. Burr, U. C. Fischer, and M. F. Garcia-Parajo, "Strong Modification of Magnetic Dipole Emission through Diabolo Nanoantennas," ACS Photonics **2**, 1071–1076 (2015).
25. A. B. Evlyukhin, S. M. Novikov, U. Zywietz, R. L. Eriksen, C. Reinhardt, S. I. Bozhevolnyi, and B. N. Chichkov, "Demonstration of magnetic dipole resonances of dielectric nanospheres in the visible region," Nano Lett. **12**, 3749–3755 (2012).
26. A. I. Kuznetsov, A. E. Miroshnichenko, Y. H. Fu, J. Zhang, and B. Luk´yanchuk, "Magnetic light," Sci. Rep. **2**, 492 (2012).
27. T. Coenen, J. van de Groep, and A. Polman, "Resonant modes of single silicon nanocavities excited by electron irradiation," ACS Nano **7**, 1689–1698 (2013).
28. L. Huang, Y. Yu, and L. Cao, "General modal properties of optical resonances in subwavelength nonspherical dielectric structures," Nano Lett. **13**, 3559–3565 (2013).
29. G. Mie, "Beiträge zur optik trüber medien, speziell kolloidaler metallösungen," Annalen der Physik **330**, 377–445 (1908).
30. F. J. García de Abajo, "Optical excitations in electron microscopy," Reviews of Modern Physics **82**, 209–275 (2010).
31. R. Sapienza, T. Coenen, J. Renger, M. Kuttge, N. F. van Hulst, and A. Polman, "Deep-subwavelength imaging of the modal dispersion of light," Nat. Mater. **11**, 781–787 (2012).
32. "Lumerical solutions, inc." .
33. E. Palik, *Handbook of Optical Constants of Solids* (Academic, 1985).
34. U. Zywietz, M. K. Schmidt, A. B. Evlyukhin, C. Reinhardt, J. Aizpurua, and B. N. Chichkov, "Electromagnetic resonances of silicon nanoparticle dimers in the visible," ACS Photonics **2**, 913–920 (2015).

1. Introduction

High-index nanoscale dielectric particles have recently attracted attention because of their ability to strongly confine and scatter light [1,2] with relatively low absorption losses, in a way that is highly tunable by the particle material and geometry [3]. The ability to concentrate, redirect and manipulate light at the nanoscale provides the ability to couple and trap light in various applications. Nanoparticles are for example used in solar cells, where they efficiently absorb and preferentially scatter light into the cell [4–9]. Alternatively, dielectric nanoparticles can be used for sensors and photo detectors of which the wavelength and polarization sensitivity can be tuned by the particle geometry [10–12].

Previous work has demonstrated that such nanoscale high-index dielectric particles support magnetic dipole (MD) and electric dipole (ED) resonances in the visible spectral range [3, 13,

#254688 Received 27 Nov 2015; revised 15 Jan 2016; accepted 16 Jan 2016; published 26 Jan 2016

14]. Interference between different resonant modes can be used to engineer the angular radiation pattern [15–17], including Kerker-type interference [18], where the scattered light is highly directional and the ratio of forward to backward scattering can be controlled [15–17]. Because of above-mentioned properties, these particles can be used as dielectric building-blocks for low-loss metasurfaces [19]. The interference of the MD and ED mode can be controlled by tuning the relative spectral position of the two modes, which can be done by changing the aspect ratio of the scattering particles [14, 17].

Here, we introduce a nanoscale resonant scattering geometry that is composed of hollow dielectric nanocylinders. In this geometry the diameter of the gap provides an additional parameter to control the wavelength and spectral distance of the MD and ED resonant modes. Furthermore, the gap provides direct access to the enhanced magnetic field of the MD mode in the center of the particle, enabling studies of the effect of the magnetic LDOS on spontaneous emission from magnetic dipole emitters such as Eu^{3+} [20–22]. So far, spontaneous emission enhancement of MD transitions have only been demonstrated using plasmonic particles [23, 24], which suffer from high losses and fabrication difficulties in the visible spectral range.

We systematically investigate the behavior of the MD and ED modes upon introducing a center gap into small dielectric Si scatterers. Careful examination of the field profiles inside the particles reveals that the MD mode is very robust to opening a 20–40 nm diameter gap in the center of a 100–150 nm diameter silicon cylinder. We experimentally study the resonant modes of hollow Si particles using cathodoluminescence (CL) spectroscopy and optical dark-field (DF) scattering. We numerically simulate the scattering spectra as a function of particle geometry. The results presented here pave the road towards designing scatterers with a highly tailored radiation pattern.

2. Optical modes in a solid dielectric nanoparticle

Before considering hollow scatterers, we will first briefly review the resonant modes in solid dielectric particles. It has been shown that small dielectric scatterers support resonant eigenmodes of which the fields are confined inside the particles, rather than on the surface, as in the case for metallic nanoparticles [3, 13, 25–28]. For spheres and infinitely long cylinders in a homogeneous medium these modes can be found from the analytical Mie solutions to Maxwell's equations [1, 29], whereas for other geometries no analytical solutions can be found. These kind of resonances are also referred to as geometrical resonances.

The optical modes supported by small dielectric particles can be either magnetic or electric in nature, where the lowest order resonances are the magnetic and electric dipole (MD and ED) modes [3, 13, 14]. The MD mode is characterized by an electric displacement current loop inside the dielectric particle, which induces a magnetic dipole moment orthogonal to the current loop (Fig. 1(a)). Since a current loop requires opposite orientation of the electric field in the top and the bottom of the particle, this MD mode can only exist in particles with sufficient retardation throughout the particle [3]. Typically, in case of Si particles, 50–100 nm particles are tall enough to couple to the opposing fields at top and bottom of the particle.

The ED mode originates from the collective polarization of the particle material in response to the external driving field. The oscillating ED induces a magnetic current loop. In this case however, the current loop can also extend outside the dielectric particle, enabling the ED mode to exist in particles which are too short to support a MD mode. The reason is that the magnetic permittivity $\mu = 1$ in both the cylinder material and the vacuum surrounding the cylinder. Fig. 1(b) shows a sketch of the ED mode together with the plane wave that can couple to this mode. High index dielectric particles with a spherical geometry have a well defined modal hierarchy, where the ED mode is found slightly blue shifted with respect to the MD mode [14]. In other geometries the relative position of the two modes can be tuned by the aspect ratio,

#254688 Received 27 Nov 2015; revised 15 Jan 2016; accepted 16 Jan 2016; published 26 Jan 2016

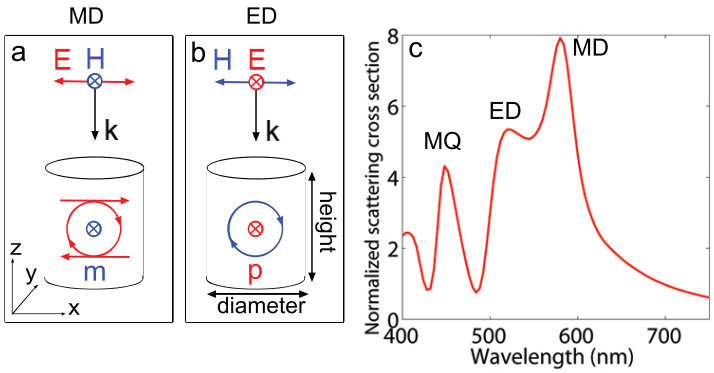

Fig. 1. Sketch of the MD and ED modes inside a solid dielectric nanoparticle. (a) The MD mode is characterized by a magnetic dipole moment as result of an electrical displacement current loop, indicated by the red circle. (b) The ED mode is the result of collective polarization of the particle material, which induces a magnetic current loop, indicated by the blue circle. The polarization of the corresponding incident plane-wave is sketched above the structures. (c) Numerically simulated normalized scattering cross section of a 100 nm tall Si cylinder with a 150 nm diameter in air. The particle is excited by a plane wave under normal incidence, as shown in (a) and (b).The MD, ED and magnetic quadrupole (MQ) modes are labeled.

which can even be designed such that the modes cross and the ED mode is found at longer wavelengths than the MD mode [17]. Introducing a gap in the center of the resonators results in an additional degree of freedom to design the spectral separation of the MD and ED mode resonances. A typical scattering spectrum of a cylindrical scatterer in air, extracted from a numerical simulation, is shown in Fig. 1(c). The peak on the red side of the spectrum corresponds to the MD mode. The ED mode appears as a shoulder on the blue side of this peak. The peak at $\lambda = 450$ nm is characterized as a magnetic quadrupole (MQ) mode [3].

In the remainder of this article, we focus on particles and substrates composed of Si, because of its high refractive index (and thus large mode confinement), relatively low absorption losses in the visible and near-IR, and well-established fabrication processes. A cylindrical particle shape is chosen because such a geometry can scatter light effectively [3], can be readily fabricated using electron beam lithography (EBL) and dry etching techniques and the resonant wavelengths can be tuned by changing the aspect ratio. We consider particles which are taller than 100 nm to be sure that the MD mode is supported. Only the lowest order magnetic (MD) and electric modes are considered in the remainder of this article. Since the field profiles of the lowest order electric mode in cylinders with a gap do not match those of an ED mode (see Section 6), we refer to the lowest order electric mode as a 'distributed electric (DE) mode' in case of hollow particles.

3. Sample fabrication

We fabricated a sample with different coax geometries on top of a Si substrate using electron beam lithography (EBL) and reactive ion etching (RIE). First we spincoat a thin layer of the negative-tone high resolution resist HSQ, for which we use a 1:2 solution of HSQ Fox-12:MIBK. Next, circles with the desired outer diameters are written with a 30 kV EBL system using a 10 μm aperture. The gap widths are controlled by changing the dose of the electron beam in the 250–1000 μC/cm^2 range, where an increased dose results in a thicker cylinder

#254688 Received 27 Nov 2015; revised 15 Jan 2016; accepted 16 Jan 2016; published 26 Jan 2016

wall. After e-beam exposure, the HSQ is developed by dipping the sample two times for 30 seconds in a 25% TMAH solution at 50°C and dried in a critical point dryer, resulting in HSQ cylinders on top of a Si substrate.

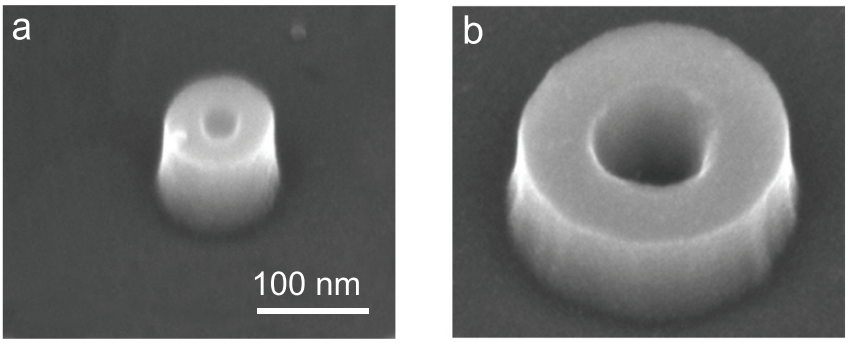

Fig. 2. SEM images of the smallest (a), having a 20 nm inner and 108 nm outer diameter, and largest (b), having a 76 nm inner and 251 nm outer diameter, Si particle on a Si substrate measured in the CL experiments. The scale is the same in both figures.

Next, the HSQ patterns are transferred into the substrate using an HBr-based RIE, which is known for its anisotropy and high selectivity for Si. After etching the samples are dipped in a 1% HF solution for 10 minutes to remove the remainders of the HSQ mask. This process results in hollow Si cylinders on a Si substrate, with a varying inner diameter in the range of 20–235 nm and outer diameter in the range of 80–250 nm. Figure 2 shows SEM images of the smallest and largest coaxes. Both particles clearly show a cylindrical shape, with only minor tapering due to the highly anisotropic RIE process.

4. Cathodoluminescence spectroscopy

Next, we study the optical scattering spectra of the fabricated cylinders using CL imaging spectroscopy. In CL, a 30 kV electron beam inside an SEM is used to locally excite the sample with a very high spatial resolution. The electric field generated by the electron beam passing through the nanoparticles coherently excites resonant modes supported by the Si nanocylinders. Since CL mainly couples to the out-of-plane component of electric fields, the excitation efficiency is sensitive to this component of the local density of optical states [30, 31]. The excited modes radiate into the far field, and the light is collected by a parabolic mirror placed between the sample and the electron column and directed to a spectrometer. A sketch of the setup is shown in Fig. 3.

In the experiment the electron beam is raster-scanned in steps of 5 nm over a single cylinder and the spectrum for each pixel is collected. At the same time the secondary electron signal is collected, such that we can match the obtained radiation spectrum with the excitation position on the sample. After correcting for the background, which is measured on an unpatterned Si surface, and the system response, we spatially average the spectrum over all positions of a single ring (including the center area). All spectra are then normalized to their maximum value.

Figure 4(a) shows the excitation as function of position on the sample at $\lambda = 500$ nm for a coaxial cylinder with an outer diameter of 170 nm and an inner diameter of 71 nm. The corresponding secondary electron image, which was taken simultaneously with the excitation

#254688 Received 27 Nov 2015; revised 15 Jan 2016; accepted 16 Jan 2016; published 26 Jan 2016

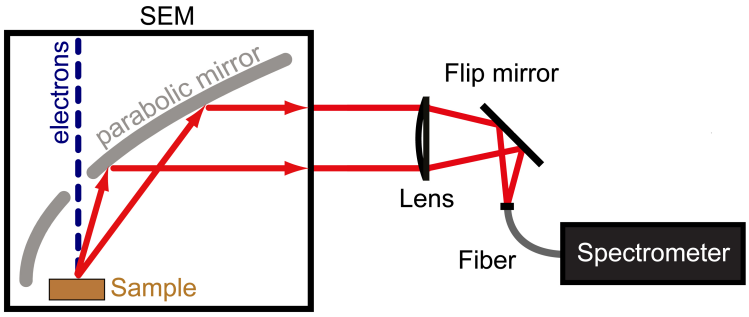

Fig. 3. Sketch of the setup used for the CL measurements. The sample is excited using a 30 kV electron beam inside a conventional SEM. The emitted light is collected by a parabolic mirror placed between the sample and the electron column and focused on an optical fiber which guides the signal to a spectrometer.

map, is shown in Fig. 4(b). We observe a bright CL ring matching with the outer circumference of the Si ring, and a dark region in the center, at the position of the gap. This excitation efficiency map is representative for all measured wavelengths and cylinders. The center is dark because the vacuum in the gap is not polarizable by the electron beam. Experimentally measured CL spectra for 122 nm tall particles are shown in Fig. 4(c), where the outer diameter of the ring is systematically increased from 108 to 251 nm. Corresponding SEM images of the smallest and largest measured rings are shown in Figs. 2(a) and 2(b), respectively. For all geometries we find clear peaks in the visible part of the spectrum. First, we observe a broad peak around 590 nm, which red shifts, broadens and decreases in intensity for increasing particle size. Second, we find two sharper peaks at shorter wavelengths, which also red shift and decrease in intensity for larger particle sizes. The red shift for these smaller peaks is less pronounced than for the broad resonance.

We use Finite-Difference Time-Domain (FDTD) simulations to obtain insight into the trends observed in Fig. 4(c) (see Section 5 for details about the simulation setup). Figure 4(d) shows the simulated scattering spectra, where the modes are excited with a plane wave under normal incidence and the power scattered in all directions is collected. A normal incident plane wave simulation can be used to find many of the resonances that can be measured with CL spectroscopy, especially in-plane modes, since both techniques can excite these modes but probe different components that are spatially separated. In-plane modes can be excited by a plane wave in the middle of a particle and by CL at the edges, where the fields are oriented out-of-plane. To get a complete overview of the resonant modes we also measured the dark field scattering spectra in Section 8.

As in the experiments, we find a broad resonance on the red side of the spectrum which shifts to longer wavelengths and decreases in intensity for increasing particle size. For small particle sizes we observe a shoulder on the blue side of the broad resonance, and for larger particles a sharp peak which red shifts at the blue side of the broad resonance. Both the shapes of the observed peaks and trends as function of particle size of the experiments are thus well reproduced by the simulations. Since the simulations match the experiments very well we will investigate the nature of the resonances and the trends as a function of particle dimensions by considering the mode profiles extracted from the simulations in the next sections.

#254688 Received 27 Nov 2015; revised 15 Jan 2016; accepted 16 Jan 2016; published 26 Jan 2016

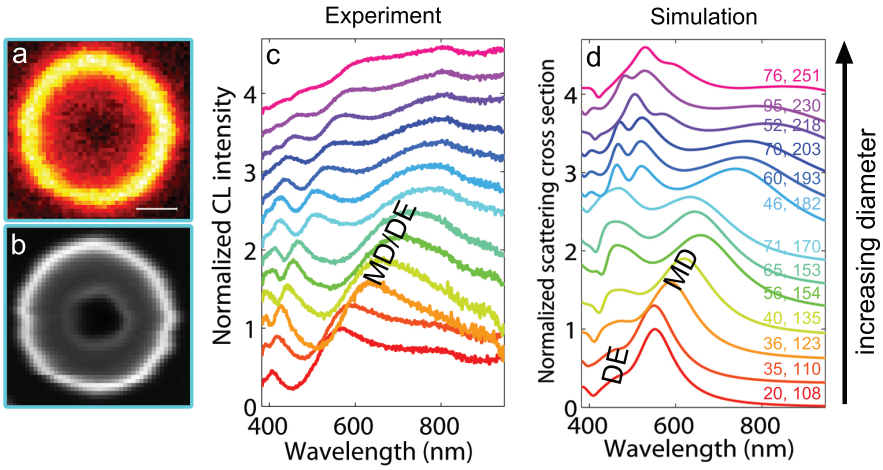

Fig. 4. CL measurements and FDTD simulations for different cylinder sizes. (a) CL excitation map of a single Si particle with an outer diameter of 170 and an inner diameter of 71 nm at $\lambda = 500$ nm. (b) Secondary electron image taken simultaneously with the CL excitation map. (c) Spatially averaged CL spectra of a Si cylinder with a height of 122 nm, for 13 different coax geometries. The particle inner and outer diameters for each spectrum is indicated by the numbers in (d), where the first number denotes the inner and the second the outer diameter, respectively. (d) FDTD simulation results of the resonant spectra in the visible, excited with a plane wave under normal incidence, using experimentally measured particle dimensions on top of a Si substrate. All spectra are normalized to their maximum value, and vertically offset for clarity.

5. FDTD simulation setup

To resolve both the resonance wavelength and the nature of the resonant modes we use Finite-Difference Time-Domain (FDTD) simulations [32]. Depending on which modes we want to excite, the particle is illuminated with a broad-band (400–750 nm) plane wave under normal incidence or at 90° incidence (by rotating the particle around the y-axis). Perfectly matching layers are used at the boundaries to prevent any unphysical backscattering from the simulation box boundaries. A refined mesh is used over the structures with a mesh size of 1–2.5 nm, depending on the dimensions of the cylinder. For the optical constants of Si we use the values determined by Palik [33]; the refractive index of the surroundings is set to 1.

A broad-band total-field scattering-field source is used to excite the sample. Power transmission monitors surrounding the particle selectively measure the power of the scattered light. The normalized scattering cross section Q_{scat}, defined as the scattering cross section divided by the area enclosed by the outer diameter of the particle, can be calculated from the scattered power. The normalization factor is thus insensitive to the size of the air gap inside the particles. The nature of the modes is resolved by using field monitors both inside and outside the particle to detect the electric and magnetic field intensities and associated current loops.

6. Modes in Si coaxes surrounded by air

In this section we numerically study the resonances supported by coaxial Si nanoparticles by considering a completely filled cylinder in which we introduce a gap with systematically increasing diameter. Here, we only consider in-plane modes of hollow cylinders in air, which are

#254688 Received 27 Nov 2015; revised 15 Jan 2016; accepted 16 Jan 2016; published 26 Jan 2016

excited with a plane wave under normal incidence, as shown in the configuration in Fig. 1.

6.1. *Simulated scattering cross section*

Figure 5(a) shows the simulated normalized scattering cross section as function of wavelength for a Si cylinder in air, with a 150 nm outer diameter and a height of 100 nm. The gap width is increased from 0 to 150 nm in steps of 10 nm. Spectra for the case of no gap (solid particle) and gap widths of 40 and 120 nm are shown in Fig. 5(b), where we find the ED resonance as a shoulder on the blue side of the MD resonance. For larger gap sizes the spectral distance between the two resonances decrease. Clearly, the peak intensities decrease for larger gap sizes.

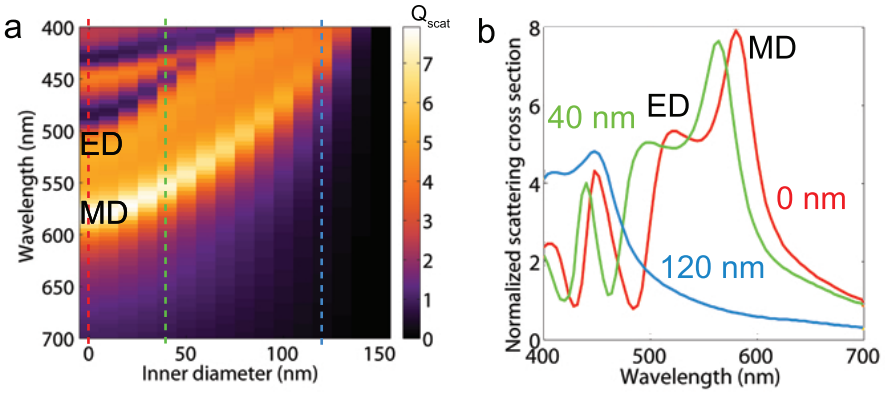

Fig. 5. Normalized scattering cross section (Q_{scat}) of a 150 nm diameter and 100 nm tall Si cylinder in air as function of wavelength and gap width in the visible wavelength range. The modes were excited with a horizontally polarized plane wave at normal incidence. In (a) the gap (inner) diameter is systematically increased from 0 (no gap) to 150 nm (no wall) in steps of 10 nm. In (b) we plot the scattering cross section as function of wavelength for three different gap sizes (0 (red), 40 (green) and 120 nm (blue)). The MD and ED modes of the particle without a gap are indicated in the spectrum. The cross sections in (b) are indicated by the dashed lines with corresponding color in (a).

As the gap inside the solid cylinders is opened, the resonant peaks gradually blue shift as result of the lower effective index experienced by the field inside the particle. The relative spectral position of both modes also changes with gap size. The spectral shift of the ED mode seems to saturate at a wavelength of ∼400 nm for an inner diameter of about 100 nm, whereas the MD mode continues to shift to shorter wavelengths for increasing gap width in the entire diameter range. This behavior is explained in Section 6.2. The resonance amplitude decreases gradually for larger gap widths, which is most pronounced for the MD resonance. This is a result of the reduced refractive index contrast as result of the reduced effective index of the particle.

6.2. *Electric and magnetic field profiles*

Next, we resolve the nature of the different modes inside hollow cylindrical Si particles in more detail by exploring their electric and magnetic field profiles. Figure 6 shows the time-averaged electric and magnetic field intensities in the *xz* and *yz* plane, as defined in Fig. 1, at the resonance wavelengths for the two lowest order modes, for the same three geometries as considered in Fig. 5(b). The electric (in case of the MD mode) and magnetic (for the ED mode) field lines are plotted as well in order to identify the corresponding current loops.

#254688 Received 27 Nov 2015; revised 15 Jan 2016; accepted 16 Jan 2016; published 26 Jan 2016

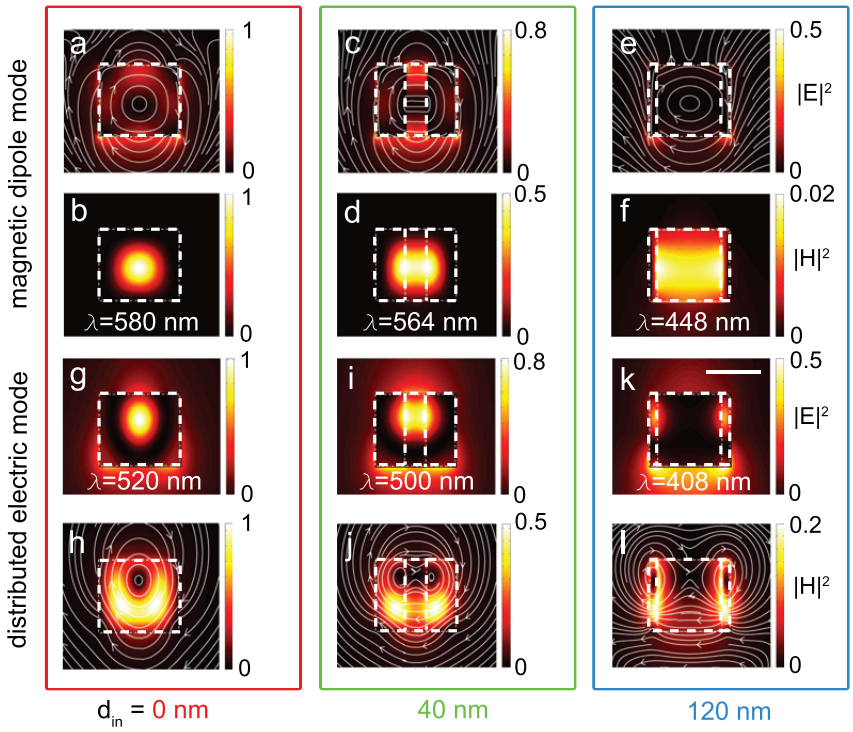

Fig. 6. Simulated electric and magnetic field profiles inside a Si nanocylinder in air. The normalized field profiles ($|E|^2$ and $|H|^2$) are plotted as cross sections through the center of the particles in the *xz* (parallel to the electric component of the driving field) (a-f) and *yz* (parallel to the magnetic component of the driving field) (h-l) planes for three different gap widths, 0, 40 and 120 nm, for the same dimensions as simulated in Fig. 5, at the wavelengths where the first two maxima in the scattering cross section are found. The peak on the red side of the spectrum is labeled the MD, whereas the peak on the blue side of the MD is labeled as the DE mode. The lines inside the field plots indicate the electric or magnetic field lines, enabling the recognition of the displacement current loops. All field intensities are normalized to the field intensities found for a solid cylinder without gap. The particle boundaries are plotted as white dashed lines. The scale bar in (k) represents 100 nm.

#254688
Received 27 Nov 2015; revised 15 Jan 2016; accepted 16 Jan 2016; published 26 Jan 2016

First we consider the MD mode of a solid cylinder without gap (a,b). We find the electric displacement current loop characteristic for the MD mode (a) and the associated enhanced magnetic field intensity in the center of the current loop (b) for the most red shifted peak in Fig. 5(b). Next, we investigate the fields inside the cylinders with a 40 nm diameter gap in the center (c,d). Again we find a clear electric current loop (c) with an enhanced magnetic field at the center of the current loop (d). Although the nature of the mode is still that of a MD mode, we notice several characteristic differences compared to the fields of a solid particle; first, the current loop is slightly deformed at the Si/air interfaces resulting in a slightly elongated shape of the magnetic field hot spot. Second, the maximum intensity of the magnetic field is about half the intensity of the enhanced field inside the particle with no gap, as can be seen from the intensity bars in Fig. 6. This is attributed to the weaker field confinement due to the lower effective refractive index of a particle with a gap.

Interestingly, if we increase the gap size even more (e,f) we can still clearly distinguish an electric current loop (e) which indicates that the electric displacement current loop can bridge a gap as large as 120 nm (the remaining Si wall thickness is just 15 nm). Considering the intensity scale bar in (f) however, we observe that the associated magnetic field intensity is only a small fraction of the enhancement observed in (b), due to the further reduced effective index of the coax.

Next, we consider the ED mode. For the particle without gap we find an enhanced electric field intensity (g) with a magnetic current loop around its center (h) as expected for the ED mode [3]. If we open the gap to 40 nm (i,j), we find two intensity maxima closely spaced next to each other inside the Si ring walls. The magnetic field lines have two centers located at the positions of the electric field maxima. This indicates a coupled electric mode, where the electric field is distributed over both sides of the cylinder walls. For the case where the gap is opened more (k,l), the electric field hot spots are further distributed over the particle walls. In this case the two electric field intensity maxima are so far apart that the electric fields only weakly overlap and no clear dipolar field profile can be recognized. The observed field profiles resemble those of a hybridized mode as found in two closely spaced dielectric nanoparticles [34]. In the presence of a gap, we will refer to the lowest order electric mode as a 'distributed electric (DE) mode' in the remainder of this article.

If we now again consider Fig. 5, we can understand why the DE mode does not shift with the same trends as the MD mode upon changing the inner diameter. Upon opening the gap the mode intensity is decreased less for the DE mode, because most of the electric field remains in the high index material of the particle. In case of the MD mode the electric current loop does extend into the gap of the particle, and is thus less confined due to a lower effective index. The magnetic field is insensitive to the field position with respect to the particle since the magnetic permeability $\mu = 1$ both inside and outside the particle. The saturation of the frequency shift of the DE mode for increasing gap width can be explained by the coupling of the two electric hot spots observed in the cylinder walls. For small gap sizes the resonance wavelength of this mode is strongly dependent on gap size as a result of strong coupling between the electric hot spots. A transition from this strongly coupled regime to a weakly coupled regime for larger gap sizes would explain the saturation of the resonant wavelength shift.

7. Influence of a Si substrate on the optical modes

The experimental and simulated data in Fig. 4 show significantly broader peaks than the simulated spectra discussed in Section 6. This is caused by the influence of the Si substrate, which is not considered in the simulations in Section 6. Simulations of the scattering cross section for Si cylinders with the same dimensions as the particles discussed in Figs. 5 and 6, but now on a Si substrate are shown in Fig. 7. As can be seen for the particle without gap (red line in (b))

#254688 Received 27 Nov 2015; revised 15 Jan 2016; accepted 16 Jan 2016; published 26 Jan 2016

the addition of a substrate results in a spectral broadening of the resonances, which causes the MD and ED modes to spectrally overlap, in agreement with the experiment. The broadening is attributed to leakage of the field into the substrate, resulting in increased radiation losses and thereby a lower quality factor of the resonant modes [7]. The broadening and spectral overlap of the ED and MD mode can be tuned by choosing a different refractive index substrate (not shown here) [3]. Furthermore, we observe a red shift of the MD resonance, which is due to the fact that a large fraction of the near-field of the resonant particle is now in the high index substrate.

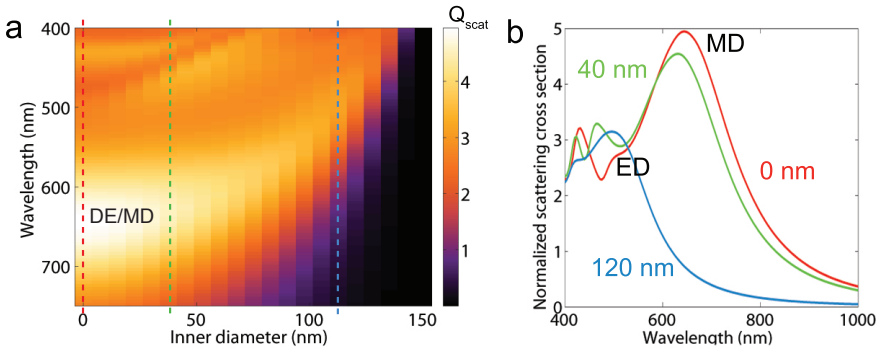

Fig. 7. Simulated normalized scattering cross section (Q_{scat}) of a 150 nm diameter and 100 nm tall Si cylinder on a Si substrate, as function of wavelength and gap width in the visible wavelength range. The modes were excited with a horizontally polarized plane wave at normal incidence. In (a) the gap (inner) diameter is systematically increased from 0 (no gap) to 150 nm (no wall) in steps of 10 nm. In (b) we plot the scattering cross section as function of wavelength for three different gap sizes (0 (red), 40 (green) and 120 nm (blue)). The peaks indicating the MD and ED resonances for the particle without gap are labeled. The geometries of the spectra in (b) are indicated by the dashed lines with corresponding color in (a).

To demonstrate this, Fig. 8 shows the fields inside the Si coaxes on a Si substrate, similar to Fig. 6. As for the particle in air, we observe an electric displacement current loop with a magnetic field intensity hot spot for the MD mode, and a magnetic current loop with an enhanced magnetic field intensity for the ED mode, as in Fig. 6. However, the MD current loops are slightly distorted. For the MD mode the current loops are shifted downwards, in agreement with the spectral broadening of the MD mode due to the extension of the mode profile into the substrate, thereby increasing the resonance linewidth. As a result, the magnetic field hot spot is also shifted into the substrate. This is important when designing an experiment where one would like to use the enhanced magnetic field intensity inside the accessible gap.

We can now label the modes of the measured resonance peaks in the CL spectra (Fig. 4(c)). CL can excite both the electric current loop of the MD mode and the horizontally polarized DE mode [27]. The MD mode can be driven by coupling the electron beam to the out-of-plane components of the electric current loop, whereas the in-plane DE mode can be driven on the particle edges, where the electric field lines have out-of-plane components. We identify the broad peak on the red side of the spectrum as the MD and DE modes. Due to the presence of the substrate, the MD and DE mode broaden and overlap. The small peaks on the blue side of the spectra are attributed to higher order modes.

#254688 Received 27 Nov 2015; revised 15 Jan 2016; accepted 16 Jan 2016; published 26 Jan 2016

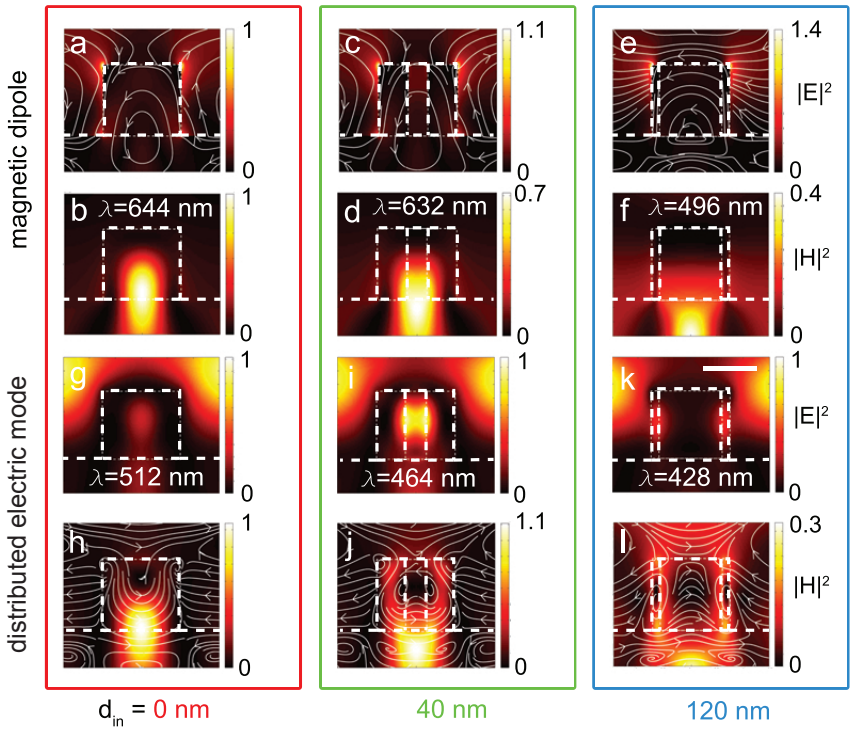

Fig. 8. Simulated electric and magnetic field profiles inside a Si nanocylinder on a Si substrate. The normalized field profiles ($|E|^2$ and $|H|^2$) are plotted as cross sections through the center of the particles in the *xz* (parallel to the electric component of the driving field) and *yz* (parallel to the magnetic component of the driving field) for three different gap widths, for the same dimensions as simulated in Fig. 7 at the wavelengths where the first two maxima in the scattering cross section are found. The lines inside the field plots show the electric or magnetic field lines, which allows for the identification of the displacement current loops. All field intensities are normalized to the field intensities found for a solid cylinder without a gap. The particle boundaries and substrate surface are plotted as white dashed lines. The scale bar (in k) represents 100 nm.

#254688
Received 27 Nov 2015; revised 15 Jan 2016; accepted 16 Jan 2016; published 26 Jan 2016

8. Dark field spectroscopy

To demonstrate the same resonant behavior under plane wave excitation, rather than electron beam irradiation, we performed DF scattering spectroscopy. The sample is excited under oblique incidence using a 50× 0.8 NA dark-field objective and a halogen lamp, and the light scattered to the top is collected by the objective. As a reference, a Lambertian isotropic scatterer is used. The measured spectra of hollow cylinders with outer diameters in the range of 138–163 nm are shown in Fig. 9(c). The measured cylinders have almost equal gap sizes.

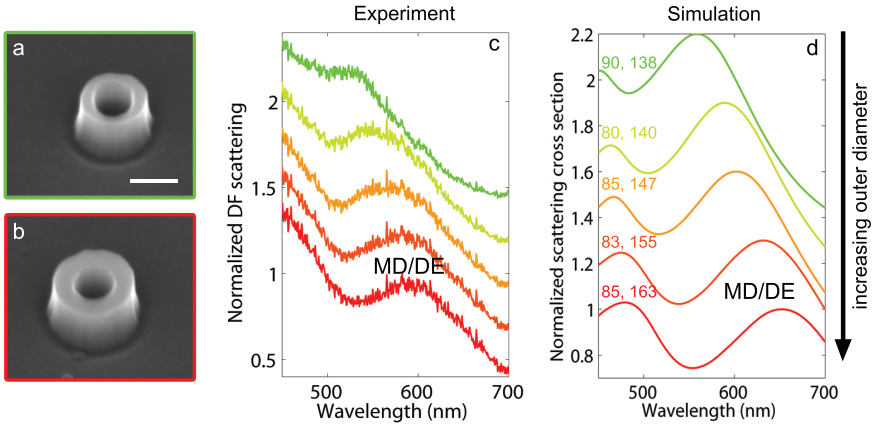

Fig. 9. DF measurements and FDTD simulations for hollow Si cylinders with different sizes. SEM images of (a) the largest and (b) smallest measured Si particle on a Si substrate. The scale bar represents 100 nm and is the same in both SEM images. (c) DF scattering spectra of a Si nanoparticle for 5 different coax geometries. The corresponding inner and outer diameters are indicated in (d), the first number denotes the inner and the second the outer diameter. The cylinders have a height of 138 nm. (d) FDTD simulations of the scattering spectra in the visible spectral range, excited with a plane wave under normal incidence of a coaxial Si particle on a Si substrate. Experimentally measured values for the particle geometries were used for the simulations. All spectra are normalized to the maximum peak value of the MD mode, and vertically offset for clarity.

Similar to Fig. 4(c), we find a broad resonance peak which red shifts with increased particle size, which we identify as an overlap of the MD and DE modes. Figure 9(d) shows the simulated scattering cross section for the same sample geometries. The simulations show the same trend as the measurements upon changing the outer diameter, but we observe that the simulated spectra are red shifted compared to the measured spectra. We attribute this to small tapering of the particles, resulting in a larger diameter on the bottom of the particles. For the simulations we used the dimensions measured on the bottom side of the cylinders. These measurements show that both the MD and DE modes can also be excited with a plane wave under oblique incidence.

9. Designing optical modes by controlling particle dimensions

The results of the previous sections show that small hollow Si cylinders support both magnetic and electric resonant modes, which can be excited experimentally with both plane waves and an electron beam. In this section, we will control several additional design parameters systematically in order to further understand the trends observed in the CL and DF measurements. Furthermore, the results of this section can be used to design experiments for which it is important to control the relative or absolute wavelength of the MD and DE resonant modes.

#254688 Received 27 Nov 2015; revised 15 Jan 2016; accepted 16 Jan 2016; published 26 Jan 2016

9.1. *Optical modes as function of outer diameter with constant gap width*

Here, we explore the behavior of the resonant modes upon changing the outer diameter of the resonators, while keeping the gap size constant. Figure 10(a) shows the normalized scattering cross section of a 100 nm tall Si particle in air as function of wavelength and outer diameter, while keeping the gap width at a constant value of 40 nm. As expected for geometric resonances, we find a red shift for both the MD and DE mode and higher order modes shifting into the visible spectral range for increasing outer diameters [2]. For increasing particle diameters the spectral separation of the MD and DE mode decreases, until they overlap, and ultimately cross at infra-red wavelengths outside the investigated wavelength range [17].

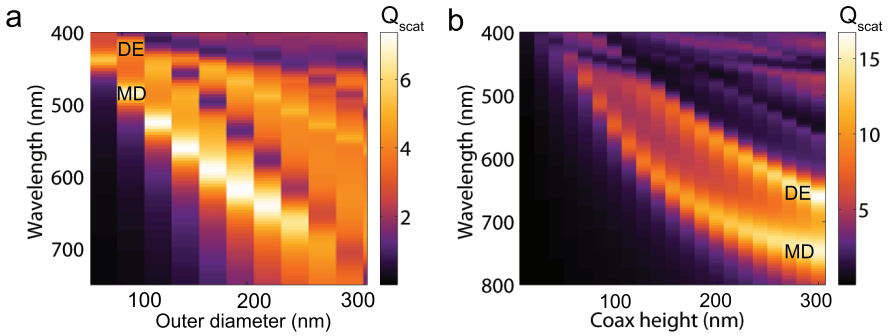

Fig. 10. Simulated normalized scattering cross section as function of wavelength for different cylinder geometries in air. The rings are excited with a plane wave under normal incidence. In (a) the outer diameter is systematically increased from 63 ?nm to 300 nm while keeping the height and inner diameter constant at 100 and 40 nm respectively. In (b) the height is systematically increased from 10 to 300 nm while keeping the inner and outer diameter constant at 40 and 150 nm respectively.

9.2. *MD and ED modes as function of particle height*

In Fig. 10(b) we explore the scattering cross section as function of the height of hollow Si cylinders in air with an inner and outer diameter of 40 and 150 nm, respectively. We find similar trends as for the solid particles, where both the MD and ED modes are red shifted, the peak intensity is increased, and higher order modes are supported by the resonators upon increased particle height [3]. The red shift is explained by the fact that a larger fraction of the electric displacement current loop can fit inside the high dielectric Si particle for increasing particle height. As seen in Fig. 10(b) the red shift starts to saturate for particles taller than $\sim$200 nm, which is the result of the current loop now fully fitting inside the particle. If the particle is too short ($<$50 nm), on the other hand, the current loop does not fit and no MD mode is observed. Since the MD and DE modes do not shift according to the same trends, changing the height and/or outer diameter of the cylinders enables control over the spectral distance between the two dipole modes. The increased scattering cross section for increasing coax height is due to the increased volume of the particle, which increases the polarizability.

9.3. *MD and ED modes as function of outer diameter with constant wall thickness*

In Section 9.1 we systematically increased the outer diameter while keeping the gap width constant. This results in similar trends as increasing the diameter for solid cylindrical particles without a gap. In this section we explore the modal behavior upon changing the outer diameter

#254688 Received 27 Nov 2015; revised 15 Jan 2016; accepted 16 Jan 2016; published 26 Jan 2016

while keeping the wall thickness (defined as the outer radius minus the inner radius) at a constant value of 40 nm. The corresponding scattering cross section as function of wavelength and outer diameter is shown in Fig. 11, where we observe several noticeable trends. For relatively small outer diameters (<150 nm) we observe a red shift of the MD mode for increasing outer diameter, which is a result of the reduced confinement due to the larger cavity diameter. Interestingly, it seems that the MD and DE modes cross at an outer diameter of ∼320 nm. Careful investigation of the mode profiles (f,g), however, shows that the field profiles at the two resonances present for a 500 nm outer diameter cylinder do not resemble the MD profile as studied before (Figs. 6(a)– 6(f)). Instead, we find a mode profile similar to the DE mode in (f), while the mode profile shown in (g) shows a higher order electric mode, with two displacement current loops in each Si wall. Considering the magnetic field profiles for a cylinder with a diameter where the modes cross (e), we find the profile of a DE mode.

Since neither of the resonances in Figs. 11(f) and 11(g) are identified as a MD mode, it suggests that this mode cannot exist for large diameter sizes, and we should thus be able to find a transition range where the MD mode disappears. Indeed, by looking at three closely spaced diameters (b,c,d) we see a gradual deformation of the displacement current loop, until the electric field lines do not form a closed loop and the MD mode disappears. This happens at a particle diameter of ∼250 nm, corresponding to a gap width of about ∼170 nm.

10. Lowest order out-of-plane electric and magnetic modes

For completeness, we also consider the vertically oriented dipolar modes. Figure 12 shows the scattering cross section of a Si cylinder in air excited with a plane wave of which the electric field is oriented along the axis of the particle. We observe two resonances, where the resonance on the red side of the spectrum is broader than the one on the blue side. Both resonances blue shift with increasing gap width. The mode on the red side of the spectrum shifts exactly the same way as in Fig. 5, indicating that this is the in-plane magnetic dipole which can be driven by both a vertically and horizontally polarized plane wave. Plotting the field profiles inside the particle (not shown here) reveals that this is indeed the in-plane MD. We note that this mode can also be driven in the CL experiments, since the electron beam can couple to the out-of-plane component of this mode.

The nature of the peak on the blue side of the MD resonance is revealed by plotting the corresponding field profiles at the resonant wavelength in the *xy* plane, as shown in Figs. 12(b) and 12(c) for a solid particle. We observe a magnetic current loop and enhanced electric field in the center, indicating an ED oriented along the long axis of the particle.

In Fig. 13 we explore the scattering behavior upon excitation with a plane wave with the magnetic field oriented along the long axis of the particle (see inset in Fig. 13(a)). For this polarization we cannot excite the in-plane MD modes as discussed in the former sections. Indeed we find that the resonance on the red part of the spectrum behaves differently upon changing the inner diameter than the MD resonance discussed in Fig. 5. Investigating the field profiles (b,c) of this mode reveals that this mode is a vertically oriented MD dipole mode, with the displacement current loop in the *xy*-plane. In Fig. 13 (a) we see that opening the gap the first 50 nm does not significantly change the MD resonance wavelength. This is explained by the fact that the electric field is mainly positioned on the outer part of the ring, as seen in (b). Opening the gap further does result in distortion of the electric field, and therefore a shift in resonance wavelength. We note that with oblique incident angles as used in the DF scattering experiment, this out-of-plane MD mode may be excited. However, the excitation efficiency is much lower than for the in-plane MD mode [34].

On the blue side of the MD in Fig. 13 we observe an in-plane DE mode which has the same scattering behavior as in Fig. 5, as confirmed by investigating the field profiles (not shown here).

#254688 Received 27 Nov 2015; revised 15 Jan 2016; accepted 16 Jan 2016; published 26 Jan 2016

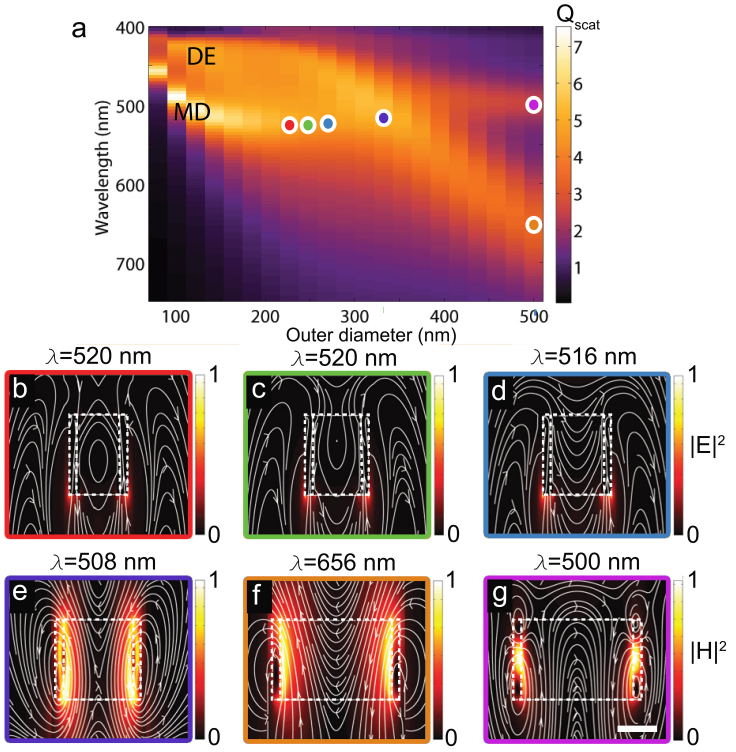

Fig. 11. Simulated normalized scattering cross section (Q_{scat}) and corresponding mode profiles of a Si cylinder on a Si substrate, having a height of 100 nm and a wall thickness of 40 nm as function of wavelength and outer diameter in the visible wavelength range. The modes were excited with a horizontally polarized plane wave at normal incidence. In (a) the outer diameter is systematically increased from 80 (no gap) to 500 nm in steps of 10 nm. (b-d) The electric fields with the corresponding electric field lines in the *xz*-plane through the center of the particles, for the wavelengths and outer diameters indicated by the red, green and blue dots in (a), representing an outer diameter of 227, 248 and 269 nm, respectively. (e-g) Show the magnetic field intensity and corresponding magnetic field lines on resonance are plotted in the *yz*-plane through the center of the particle, for outer diameters of 332 (crossing point) and 500 nm. The colors of the dashed lines drawn in (a) indicate the geometries of the plotted fields in (b-g). The scale bar in (g) represents 150 nm.

#254688 Received 27 Nov 2015; revised 15 Jan 2016; accepted 16 Jan 2016; published 26 Jan 2016

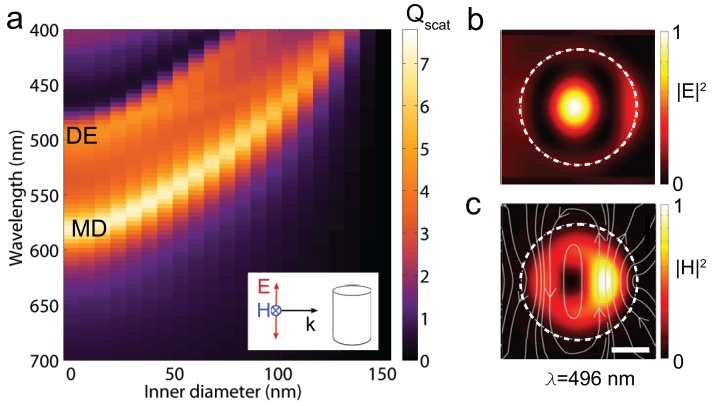

Fig. 12. Simulated normalized scattering cross section (Q_{scat}) of a 150 nm diameter and 100 nm tall Si cylinder in air, as function of wavelength and gap width in the visible wavelength range. The modes were excited with a vertically polarized plane wave (with the E-field along the long axis of the particle), as seen in the inset of (a). The normalized electric (b) and magnetic (c) field intensity profiles for a solid particle with no gap with the corresponding electric field lines are shown for the xy-plane in the center of the particle on resonance, where the particle contour is plotted as white dashed lines. The field intensities are normalized to its maximum values. The scale bar in (c) represents 50 nm.

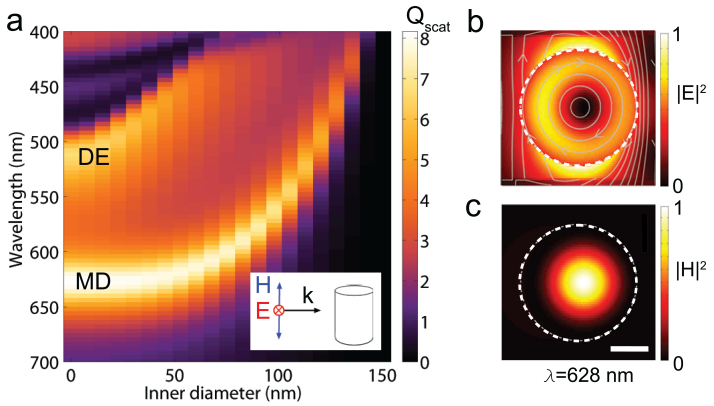

Fig. 13. Simulated normalized scattering cross section (Q_{scat}) of a 150 nm diameter, 100 nm tall Si cylinder in air, as function of wavelength and gap width in the visible wavelength range. The modes were excited with a vertically polarized plane wave (with the H-field along the long axis of the particle), as seen in the inset of (a). The electric (b) and magnetic (c) field intensity profiles at $\lambda = 628$ nm, for a particle without gap with the corresponding electric field lines are shown for the xy-plane in the center of the particle, where the particle contour is plotted as white dashed lines and the fields are normalized to the maximum. The scale bar represents 50 nm.

#254688
Received 27 Nov 2015; revised 15 Jan 2016; accepted 16 Jan 2016; published 26 Jan 2016

11. Conclusion

We have systematically explored the geometrical optical resonances supported by hollow Si nanocylinders. We fabricated such resonant structures with an outer diameter of 108–251 nm and a gap size >20 nm using EBL. The resonant modes are measured using CL spectroscopy and DF scattering spectroscopy. Using numerical simulations, we resolve the nature of the modes and show that introducing a <40 nm gap in the center of a 100–250 nm outer diameter silicon cylinder results in only small deviations from the well known ED and MD geometrical resonances of solid cylinders. For larger gap sizes the nature of the MD mode is preserved up to gap widths of 190 nm, while the lowest order electric mode becomes strongly localized in the opposing Si walls. We show that the resonant wavelength and relative spectral spacing of the modes can be controlled by changing the outer diameter, height and wall thickness of the hollow cylinders. Compared to solid cylinders, the gap size comprises an additional design parameter to tune the relative spectral spacing. Furthermore, we find that the introduction of a Si substrate significantly broadens the resonances and influences the position of the magnetic field intensity hotspot of the MD mode.

Acknowledgments

This work is part of the research program of the Stichting voor Fundamenteel Onderzoek der Materie (FOM), which is financially supported by the Nederlandse Organisatie voor Wetenschappelijk Onderzoek (NWO). It was also funded by NanoNextNL, a technology program of the Netherlands Ministry of Economic Affairs and the European Research Counsel. A.P. is co-founder and co-owner of Delmic BV, a startup company developing a commercial product based on the cathodoluminescence system that was used in this work.

#254688 Received 27 Nov 2015; revised 15 Jan 2016; accepted 16 Jan 2016; published 26 Jan 2016